RESEARCH ARTICLE

Design and analysis of high birefringence and nonlinearity with small confinement loss photonic crystal fiber

Rekha SAHA, Md. Mahbub HOSSAIN (✉), Md. Ekhlasur RAHAMAN, Himadri Shekhar MONDAL

Electronics and Communication Engineering Discipline, Khulna University, Khulna 9208, Bangladesh

Abstract High birefringence with low confinement loss photonic crystal fiber (PCF) has significant advantages in the field of sensing, dispersion compensation devices, nonlinear applications, and polarization filter. In this report, two different models of PCFs are presented and compared. Both the models contain five air holes rings with combination of circular and elliptical air holes arrangement. Moreover, the elliptical shaped air holes polarization and the third ring air holes rotational angle are varied. To examine different guiding characteristics, finite element method (FEM) with perfectly matched layer (PML) absorbing boundary condition is applied from 1.2 to 1.8 μm wavelength range. High birefringence, low confinement loss, high nonlinearity, and moderate dispersion values are successfully achieved in both the PCFs models. Numeric analysis shows that model-1 gives higher birefringence (2.75×10^{-2}) and negative dispersion (-540.67 ps/(nm·km)) at 1.55 μm wavelength. However, model-2 gives more small confinement loss than model-1 at the same wavelength. In addition, the proposed design demonstrates the variation of rotation angle has great impact to enhance guiding properties especially the birefringence.

Keywords birefringence, dispersion, polarization maintaining, photonic crystal fiber (PCF), polarization-selective devices, polarization

1 Introduction

Today's telecommunication system strongly depends on data based communication like different online based services, video communication, video sharing, and many more. The rate of increment of this data demand is raising

exponentially. Research is going on to enhance the data capacity of optical fiber in the most recent years [1–4]. As a candidate, photonic crystal fiber (PCF) has a great field of attraction to the researchers [5,6]. PCFs are made up of central core of solid silica or air and periodic arrangement of air holes throughout the length. PCFs have many usual optical properties like endless single mode operation [3,7], high birefringence [8–10], dispersion compensation [11,12], large mode area [13–15], and high nonlinearity [16] over the conventional fiber. This is the main reason of using PCFs which is the major topic in the area of optical fiber research.

Dispersion, confinement of light, and birefringence are the most important properties of PCF. Practically, these properties are used in bio-medical and medical diagnostic, telecommunication, and sensing applications [17–19]. Dispersion management of PCFs is very much vital due to significant variation of different methods [20]. PCFs offer higher birefringence than conventional fibers due to large index difference. Asymmetric design or various air hole geometries of PCFs support high birefringence [21–23]. Usually to increase the birefringence, rupture the steadiness of the structures and create refractive index variation involving the two orthogonal polarization states [24]. The elliptical air holes arrangement in PCFs confirm fully complicated fabrication procedures [25–27]. Though it is well established that non-circular air holes like elliptical are difficult to fabricate but it is applied to obtain high birefringence [28,29]. Nonetheless, the shape and size of the elliptical air holes require a conscientious control in the fabrication procedures [30]. Also, stack and draw fabrication methods provide an enormous birefringence to be appreciated on PCFs.

High birefringence is introduced by elliptical air hole PCFs (EHPCFs) which shows birefringence of 1.12×10^{-2} that is bigger than the traditional fiber (5×10^{-4}), circular PCF (3.7×10^{-3}), and elliptical shape hollow PCF (EHPCF) (2.35×10^{-3}) [27]. To increase the birefringence, an imitation imperfections spiral PCF (S-PCF) is proposed

which shows birefringence of 0.09 at the excitation wavelength 1.55 μm [31]. An asymmetrical structure is made by using circular air holes at the cladding region and elliptical air holes at the core region that shows birefringence up to 10^{-2} [30]. A hybrid PCF (HyPCF) is proposed to achieve birefringence of 1.77×10^{-2} and confinement loss is less than 10^{2} dB/km at 1.55 μm wavelength [32]. Hasan et al. proposed an equiangular spiral photonic crystal fiber (ES-PCF) which gives a usual negative dispersion of 526.99 ps/(nm·km) from 1.05 to 1.70 μm wavelength and large birefringence of 0.026 at 1.55 μm wavelength [33]. Moreover, modified octagonal PCF (M-PCF) is proposed that demonstrated birefringence of 1.81×10^{-2} at 1.55 μm wavelength [34]. However, these types of PCFs show highly fabrication complexity especially elliptical air holes at the core region.

To enhance the birefringence, another report proposed increasing the diameter of the center air holes which provides 1.4×10^{-3} birefringence at 1.55 μm wavelength [35]. At 1.55 μm wavelength, the birefringence of 8.7×10^{-3} is observed for index-guiding PCF applying the complex unit cells in cladding [24]. A hybrid PCF is presented which shows high dispersion of -242.22 to -762.6 ps/(nm·km) and 0.0264 birefringence at 1.55 μm wavelength [36]. Another report proposed a dispersion compensation PCF (DC-PCF) design with a negative dispersion from -388.72 to -723.1 ps/(nm·km) in the telecommunication bands for broadband dispersion compensation with a birefringence and nonlinear coefficient of 3.79×10^{-2} and 40.1 $W^{-1} \cdot km^{-1}$ at 1.55 μm wavelength [37]. One more report demonstrated high birefringence of 5.501×10^{-3} with low confinement loss 7.30×10^{-5} dB/km at 1.55 μm wavelength supported by single rectangular midpoint ring of minor rounded air holes in the fiber core [38]. Moreover, at 1550 nm wavelength the maximum birefringence of 0.87×10^{-2} with confinement loss less than 0.01 dB/km is proposed by Ref. [39]. However, the guiding properties of these models especially the dispersion values are comparatively small at 1.55 μm wavelength. Also, the birefringence did not follow a constant value over a broad

wavelength range. As a result, the fiber length and production cost increase. Moreover, different broadband DC-PCFs have been considered but none of them has provided birefringence value more than 2.1×10^{-2} [34,40,41]. Recently, a highly birefringence solid core PCF through asymmetric cladding is proposed (elliptical air hole) which presents birefringence of 8.56×10^{-3} at 1.55 μm wavelength but the dispersion value is not satisfactory [42].

In the proposed design, a high birefringence and low confinement loss PCFs with asymmetric design from 1.2 to 1.8 μm wavelength are analyzed. By using circular air holes in the first two rings and elliptical air holes for the remaining rings through different rotation angle show significant asymmetry in the cladding region. Moreover, two circular air holes are omitted from the core region to increase the light confinement. The proposed models present higher birefringence due to introduce the asymmetry in the cladding region. In addition, high negative dispersion, small effective mode area, and high nonlinear coefficient are presented.

2 Materials and methods

2.1 Designing methodology

Figure 1 shows the cross section of the proposed PCFs which is designed using the combination of circular and elliptical air holes in the cladding. The proposed PCFs contain five air hole rings where first two circular air hole rings are hexagonal with diameter d_1 and other three air holes rings are elliptical shaped. The core of the PCF is formed by eliminating two air holes of the first hexagonal air hole ring in the horizontal direction where the mode field is well confined in the core region. The total number of circular air holes on the 1st and 2nd rings are respectively 4 and 12. Usually circular air holes rings are rotated to obtain high birefringence [37]. In this report, the rotation angle of elliptical air holes on the 3rd, 4th and 5th
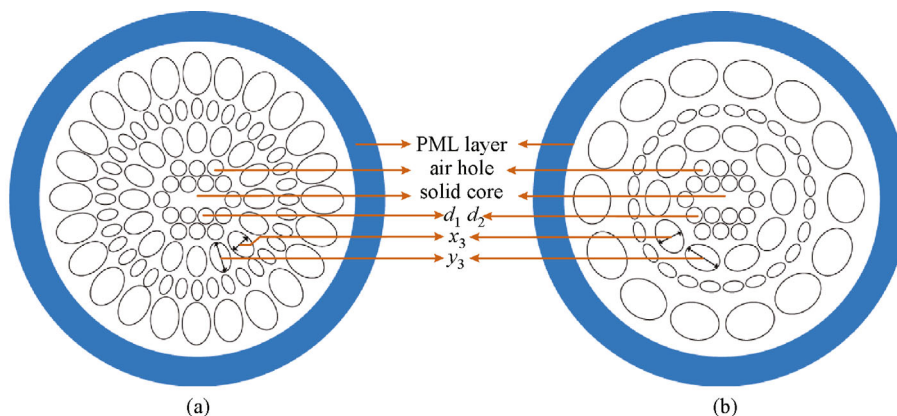

Fig. 1 Cross-section of the proposed PCFs. (a) Model-1; (b) model-2

rings are 22.5°, 10° and 15° for model-1 and 36°, 16.36° and 25.71° for model-2, respectively. Moreover, to identify the effect of angle rotation on PCF guiding properties, the third ring rotation angle is varied. Mainly rotation angle determine the number of air holes in the cladding area. As rotation angle = 360°/number of air holes in the cladding region, then taking rotation angle as 26° in the 3rd elliptical air hole ring the number of air holes in the cladding is 13.84 which is a frictional number and usually air holes value cannot be fractional. As elliptical air holes are taken 15, 16 and 17 which is the reason behind to take rotation angle 21.18°, 22.5° and 24°.

In the proposed design, the corresponding PCF as model-1 for Fig. 1(a) and model-2 for Fig. 1(b) is shown. In model-1 and model-2, the value of d_1 and d_2 is 0.83 and 0.807 μm and distance between two air holes is 0.85 μm. In the same manner x_3 and y_3, x_4 and y_4, and x_5 and y_5 denote the two axes of elliptical air holes along the x and the y-direction. The values of x_3 and y_3, x_4 and y_4, and x_5 and y_5 are taken respectively as 0.75 and 0.5 μm, 0.5 and 0.25 μm, and 1 and 0.75 μm for both the models. The rotation angle of 3rd elliptical air hole ring is varied as 21.18°, 22.5°, and 24° for model-1 and 32.72°, 36°, and 40° for model-2, respectively. Moreover, the difference between model-1 and model-2 is the position of elliptical air hole. In model-1, elliptical air holes are organized in vertical direction whereas in model-2 the air holes are horizontal direction. The modal analysis is done by applying finite element method (FEM-Comsol Multi-physics. version 5.2) from 1200 to 1800 nm with 10 nm wavelength increments united with perfectly matched layer (PML) boundary condition.

2.2 Theoretical analysis

The modal properties of the proposed fiber are simulated and analyzed by using FEM [43]. Energy loss can be minimized by using PML and a scattering boundary condition [44]. Refractive index of the back-ground material depends on wavelength and can be obtained by using Sellmeier formula [45,46]

$$n(\lambda^2) = 1 + \frac{B_1\lambda^2}{\lambda^2 - l_1} + \frac{B_2\lambda^2}{\lambda^2 - l_2} + \frac{B_3\lambda^2}{\lambda^2 - l_3}, \quad (1)$$

and the generalized equation can be written as

$$n(\lambda^2 - 1) = \sum_{i=1}^{j} \frac{B_i\lambda^2}{\lambda^2 - l_i^2}, \quad (2)$$

where $j = 3$, $B_1 = 0.6961663$, $B_2 = 0.4079426$, $B_3 = 0.8974794$, $l_1 = 0.0684043$ μm, $l_2 = 0.1162414$ μm, and $l_3 = 9.896161$ μm, λ is the operating wavelength, and $n(\lambda)$ is the wavelength-dependent refractive index. From Maxwells curl equation, the vectorial equation can be written as follows [47]

$$\nabla \times ([s]^{-1}\nabla \times E) - k_0^2 n^2 [s]E. \quad (3)$$

Here, E is the electric field vector, $k_0 = \frac{2\pi}{\lambda}$ is the wave number in the vacuum, $[s]^{-1}$ is an inverse matrix of $[s]$, and n_{eff} is effective refractive index given as $n_{\text{eff}} = \frac{\beta}{k_0}$, where β is the propagation constant. The effective refractive index difference of the two fundamental modes is defined as birefringence which can be calculated through the following relation [48]

$$B = |(n_x - n_y)|, \quad (4)$$

where n_x and n_y are the effective refractive indices of the two-orthogonal polarization fundamental modes. All power do not propagate through the core region and some power emits through the air holes that arises confinement loss. Calculation of confinement loss requires imaginary part of effective refractive index of modes and can be calculated by using the following equation [49,50].

$$L = 8.686 \times \frac{2\pi}{\lambda}\text{Im}(n_{\text{eff}}) \times 10^3 \text{ dB/km}, \quad (5)$$

where $\text{Im}(n_{\text{eff}})$ is the imaginary part of the refractive index of the propagating mode. Through the following relation, dispersion can be calculated [51].

$$D(\lambda) = -\frac{2\pi c}{\lambda^2}\beta \simeq -\frac{\lambda}{c}\frac{d^2 n_{\text{eff}}}{d\lambda^2}, \quad (6)$$

where c is the speed of light in vacuum. The value of the effective area and nonlinear coefficient can be obtained by the following formula [52]

$$A_{\text{eff}} = \left(\iint |E|^2 dxdy\right)^2 / \iint |E|^4 dxdy, \quad (7)$$

$$\gamma = \left(\frac{2\pi}{\lambda}\right)\frac{n_2}{A_{\text{eff}}}, \quad (8)$$

where n_2 is nonlinear refractive index coefficient of silica.

3 Results and discussion

Figure 2 demonstrates the optical field distribution of the fundamental mode of the proposed PCFs. The rotation angle of elliptical air hole on 3rd ring is 22.5° for model-1 and 36° for model-2 at $\lambda = 1.4$ μm wavelength. Figure 2 also illustrates the mode field in model-1, is strongly confined than the other one. For the reason of small rotational angle of model-1 which increases the number of elliptical air holes on third ring. Therefore, the light is strongly confined in the core region. The dark red color indicates the strong confinement of light in the core region. Moreover, high color density represents the high intensity of absorption. The figure also illustrates the optical field
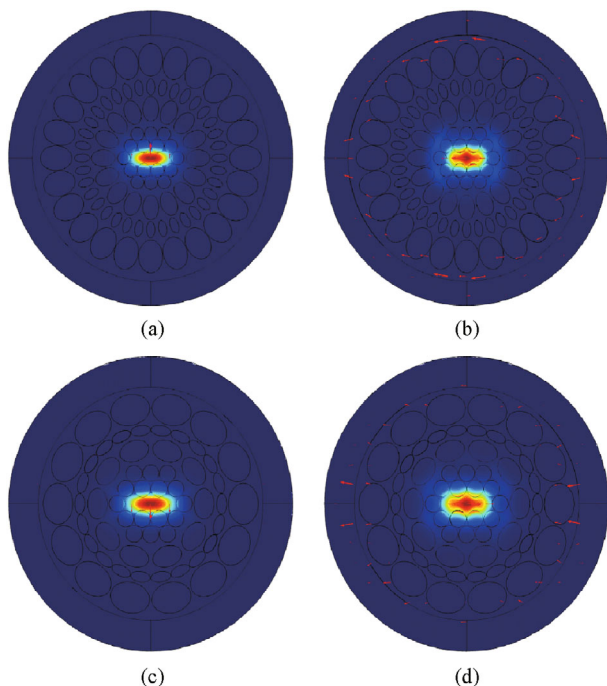
Fig. 2 Optical field distribution of the proposed PCFs. (a) *x*-polarization, (b) *y*-polarization for model-1; (c) *x*-polarization, (d) *y*-polarization for model-2

that extends broadly in the direction of *x*-axis than *y*-axis due to adequate space given in the *x*-direction by omitting the air holes.

Figure 3 represents the variation of effective index (real) for the proposed PCF model-1 with respect to wavelength for both *x*- and *y*-polarization. For both the polarizations, with the increase of the wavelength, the effective index is decreased. Higher effective index is observed at *y*-polarization with all the three rotational angle. At 1.55 μm wavelength, the effective index difference is 0.0275, 0.0145, and 0.0075 for 21.18°, 22.50°, and 24.00°, correspondingly. As small rotational angle 21.18° shows
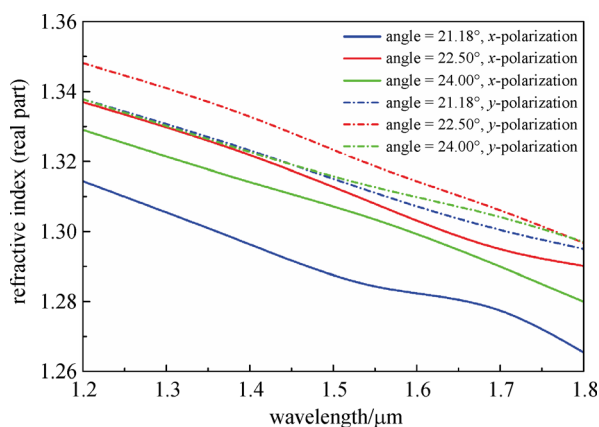
higher index difference then it gets the high birefringence.

Figure 4 shows the variation of effective refractive index (real) for the proposed PCF model-2 with respect to wavelength for both *x*- and *y*-polarization. For both the polarizations increasing wavelength the effective index is decreased, as usual. Moreover, higher effective index is observed for *y*-polarization of all the three rotational angles. At 1.55 μm wavelength, the effective index difference is observed 0.0115, 0.0116, and 0.0101 for 32.72°, 36.00°, and 40.00°, correspondingly. Model-2 represents slightly different result than model-1 at 1.55 μm. At this specific wavelength, the effective index difference is higher for 36.00° rotational angle not 32.72°. Increasing wavelength from 1.2 to 1.8 μm, the effective index reduction rate is shown 4.60%, 4.65%, 3.76% for *x*-polarization, and 5.01%, 5.13%, and 4.33% for *y*-polarization with the three rotational angles, respectively. However, this reduction rate is observed 3.42%, 5.90%, 3.21% for *x*-polarization, and 4.03%, 4.75%, and 3.88% for *y*-polarization, respectively of model-1.

Figure 5 shows the variation of effective refractive index (imaginary part) for the proposed PCF model-1 and model-2 with respect to wavelength for *x*-polarization only. Generally, with the increase of the wavelength, the effective imaginary index raises. From 1.2 to 1.5 μm wavelength range, the imaginary index shows very small. After 1.5 μm wavelength, the imaginary part is increased upward. Moreover, the lowest imaginary index is obtained at 36° with model-2 at 1.55 μm wavelength. Also, at 1.55 μm wavelength, model-2 exhibits the highest imaginary index at 40° rotational angle.

The birefringence is calculated through the effective refractive index difference of the fundamental guided modes. Figure 6 exhibits the birefringence with respect to wavelength for PCF model-1. The maximum birefringence of 2.75×10^{-2} is obtained at 21.18° rotational angle. However, from 1.4 to 1.55 μm wavelength range, this high

Fig. 3 Refractive index (real part) with respect to wavelength for proposed PCF model-1
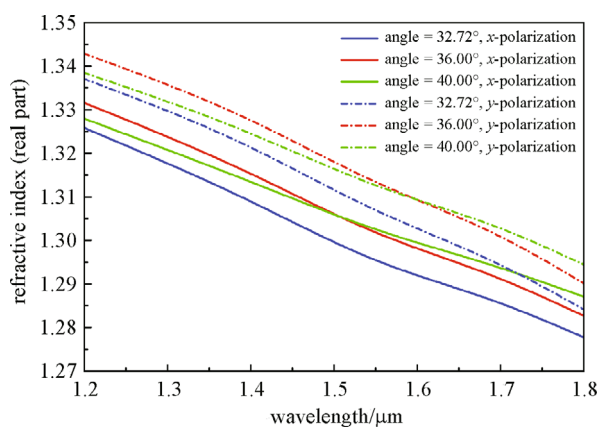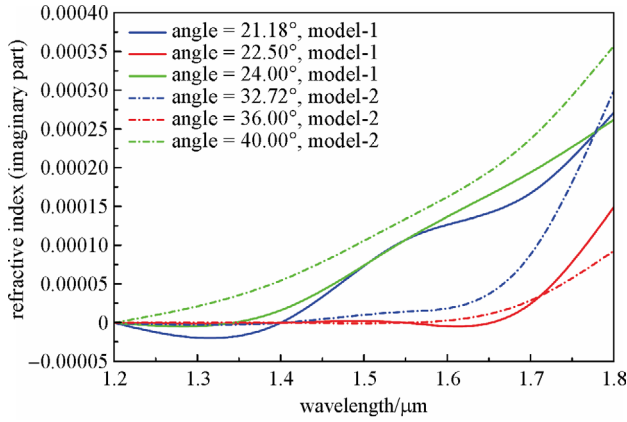

Fig. 4 Refractive index (real part) with respect to wavelength for proposed PCF model-2

Fig. 5 Refractive index (imaginary part) with respect to wavelength for proposed PCF model-1 and model-2

Fig. 6 Birefringence with respect to wavelength for proposed PCF model-1
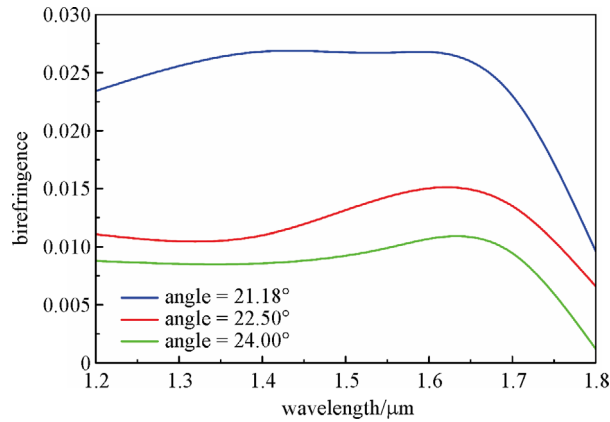

Fig. 7 Birefringence with respect to wavelength for proposed PCF model-2

constant birefringence is observed. However, with the increase of the rotational angle, the birefringence reduces significantly. This is due to decrease the effective index difference of x- and y-polarizations as shown in Fig. 3. Moreover, the birefringence is gradually decreased with all the three rotational angle for 1.55 to 1.8 μm wavelength range. Birefringence actually depends on structural asymmetry. In the proposed design, the structural asymmetry is achieved by introducing elliptical air holes in the cladding region as well as by changing rotation angle of air holes in the third ring. Changing rotation angle or number of air holes, then the structural asymmetry will change which will lead to enhance birefringence.

Figure 7 illustrates the results of birefringence with wavelength for model-2. The maximum birefringence of 1.29×10^{-2} is obtained at 32.72° rotational angle at 1.45 μm wavelength range. However, with the increase of the rotational angle, the birefringence reduces similarly to model-1. Interestingly, at 1.55 μm wavelength, 36.00° rotational angle gives the highest birefringence. Increasing
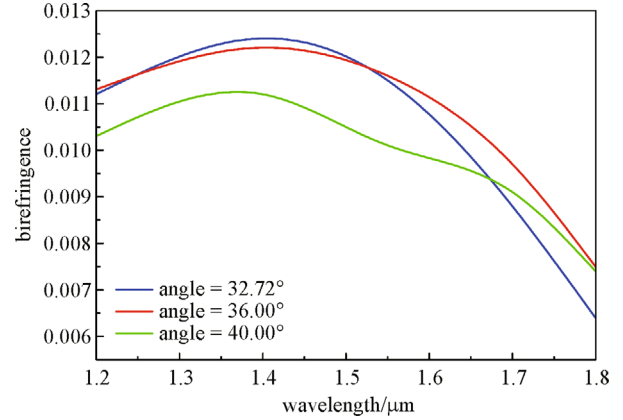
wavelength, birefringence is decreased for all the rotational angle due to reduce the effective index difference of x- and y-polarizations as shown in Fig. 4. Thus, model-1 gives the higher birefringence than model-2 with smaller rotational angle.

Figures 8 and 9 exhibit the effect of rotation angle of elliptical air hole on 3rd ring to the dispersion behavior when the other parameters are kept constant for model-1 and model-2, respectively. Figure 8 shows the rotational angle of 21.18°, 22.50°, and 24.00°, the dispersion at 1.55 μm are –300.074, –399.185 and –536.296 ps/(nm·km), respectively. However, the maximum dispersion –955.25, –650.98, and –625.56 ps/(nm·km) are obtained in 1.8, 1.7, and 1.45 μm wavelength for the three rotational angle. Though, it is observed that 24.00° rotational angle shows maximum dispersion from 1.4 to 1.55 μm wavelength range, it gives the lowest birefringence at the specific wavelength range. However, changing the structure parameters, these guiding properties can be enhanced.

Figure 9 demonstrates the dispersion variation with wavelength for proposed model-2. The dispersion varia-
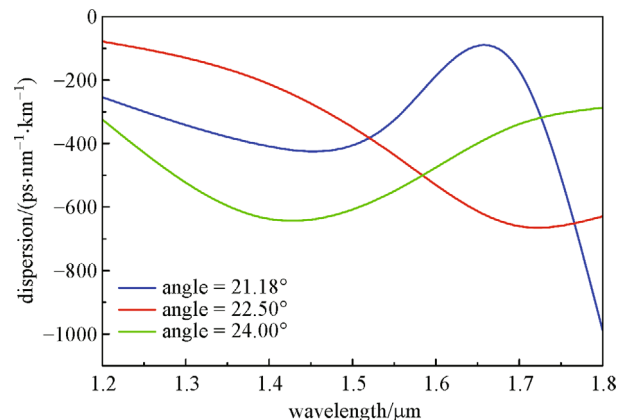

Fig. 8 Dispersion with respect to wavelength for proposed PCF model-1, x-polarization
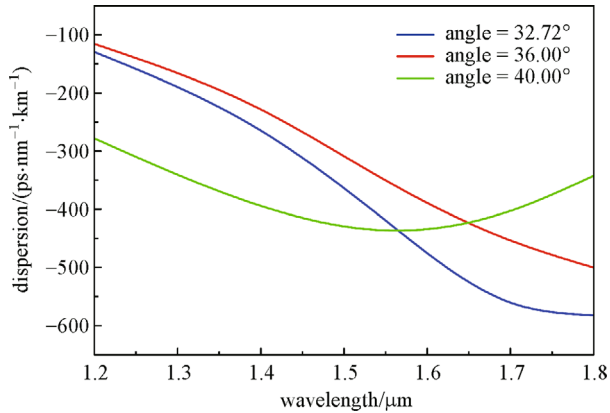
Fig. 9   Dispersion with respect to wavelength for proposed PCF model-2, *x*-polarization

Fig. 11   Confinement loss with respect to wavelength for proposed PCF model-2

tion is observed –110 to –575 ps/(nm·km). The maximum dispersion is achieved from 1.4 to 1.55 μm wavelength range at 40.00° rotational angle which usually shows the minimum birefringence. Increasing wavelength negative dispersion is usually increased, though 40.00° rotational angle shows the lowest dispersion variation comparing to other rotational angles. Therefore, it can be concluded that rotational angle has great impact on dispersion and birefringence.

Figures 10 and 11 depict the difference of confinement loss with wavelength for model-1 and model-2, respectively. Simulation results imply that with the increase of wavelength confinement loss is increased and this increment is more severe at the higher wavelength range. Lowest confinement loss is achieved at 22.50° and 36.00° rotational angle for both the models. However, model-2 shows comparatively small loss than model-1 at higher wavelength. In addition, both the models show higher loss at higher rotational angle. Because at higher rotational angle, light is not strongly confined in the core. However, the proposed models represent smaller confinement loss compared to the exiting work [32,53].
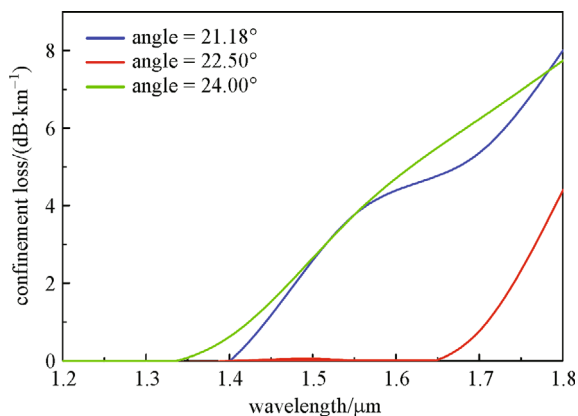
The effective area is shown in Figs. 12 and 13 for model-1 and model-2, respectively against wavelength. Effective area increases with wavelength in both the models. For both the PCFs minimum effective area is observed at 22.50° or 36.00° rotational angle. For model-1, the effective area variation is almost constant from 1.6 to 1.8 μm wavelength range. However, increasing wavelength after 1.4 μm there is a large variation of effective area depending on rotational angle for model-1. The similar trend is observed for model-2 though 40.00° rotational angle which shows the maximum effective area at higher wavelength. However, the effective area is almost unvaried (model-2) in the lower wavelength range for the others two rotational angles.

Figures 14 and 15 show the variation of nonlinear coefficient with respect to wavelength. In both the models, with the increase of the wavelength nonlinear coefficient decreases. At 1.55 μm wavelength, the maximum nonlinear coefficient 43.7 and 41.98 $W^{-1}\cdot km^{-1}$ are observed at 22.50° and 36.00° rotational angle, respectively for both the models. Noted that model-1 shows maximum nonlinear coefficient at low wavelength whereas model-2 represents
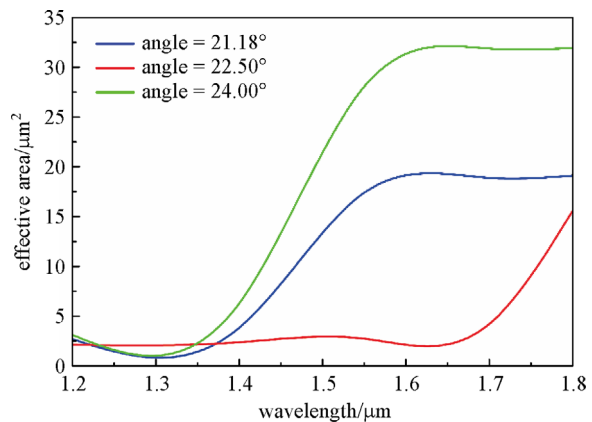

Fig. 10   Confinement loss with respect to wavelength for proposed PCF model-1

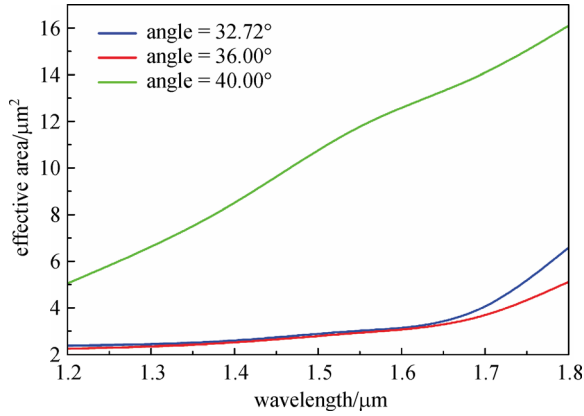**Fig. 12**   Effective area with respect to wavelength for proposed PCF model-1

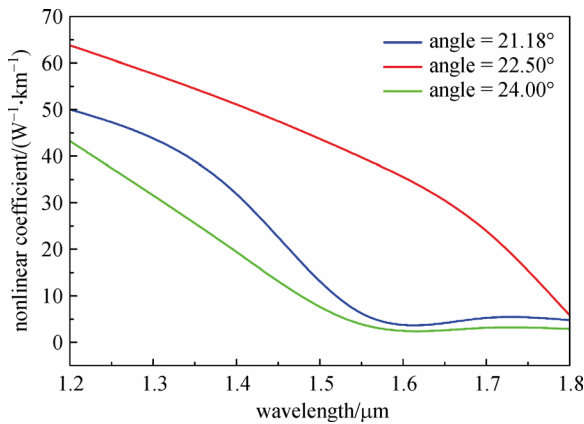**Fig. 13** Effective area with respect to wavelength for proposed PCF model-2

Fig. 14 Nonlinear coefficient with respect to wavelength for proposed PCF model-1
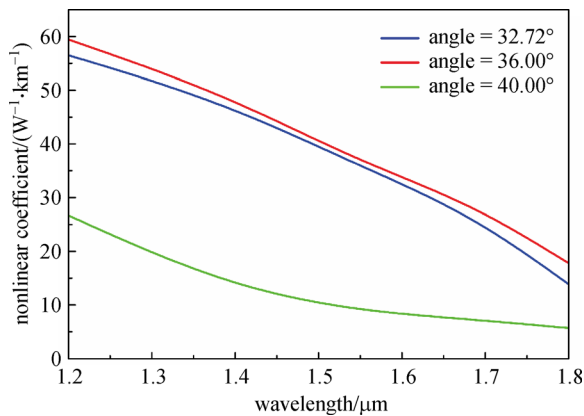

Fig. 15 Nonlinear coefficient with respect to wavelength for proposed PCF model-2

maximum nonlinear coefficient at high wavelength. Therefore, rotational angle shows great impact on different guiding properties.

Fabrication possibility is a leading apprehension in designing PCFs. The fabrication progression of elliptical shape PCFs can be vulnerable to fall down and to alter into circular shape for the surface tension. Bunches of PCFs fabrication methods are offered at the present time resembling drilling, die cast, extrusion, stack and draw, sol-gel. Newly, Liu et al. have been made-up mixed air hole diameters at the cladding area by using the usual stack and draw method [54]. Moreover, multi-step method of creating perform is presented by Falkenstein et al., where elliptical PCFs model were tested in practically [55].

4 Conclusion

An ultra-high birefringence with moderate negative dispersion and negligible confinement loss PCFs have been proposed. Also, effective area and nonlinear coefficient have been investigated. Numeric analysis shows highly birefringence of 2.75×10^{-2} with moderate dispersion at 1.55 μm wavelength. Rotating the angle on the third ring of the elliptical air holes has significant impact on the various guiding properties. Results also imply that model-1 shows maximum birefringence whereas model-2 represents low confinement loss. This reported results can be widely applicable in sensing applications, polarization, and long distance data transmission.

References

1. Knight J C, Russell P S J. New ways to guide light. Science, 2002, 296(5566): 276–277
2. Knight J C, Birks T A, Russell P S J, Atkin D M. All-silica single-mode optical fiber with photonic crystal cladding. Optics Letters, 1996, 21(19): 1547–1549
3. Birks T A, Knight J C, Russell P S J. Endlessly single-mode photonic crystal fiber. Optics Letters, 1997, 22(13): 961–963
4. Knight J C, Broeng J, Birks T A, Russell P S J. Photonic band gap guidance in optical fibers. Science, 1998, 282(5393): 1476–1478
5. Russell P. Photonic crystal fibers. Science, 2003, 299(5605): 358
6. Russell P, Dettmer R. A neat idea [photonic crystal fibre]. IEE Review, 2001, 47(5): 19–23
7. Sinha R K, Kumar A, Saini T S. Analysis and design of single-mode As_2Se_3-chalcogenide photonic crystal fiber for generation of slow light with tunable features. IEEE Journal of Selected Topics in Quantum Electronics, 2016, 22(2): 287–292
8. Mishra S, Singh V K. Study of the fundamental propagation properties of a solid core holey photonic crystal fiber in the telecommunication window. Zhongguo Wuli Xuekan, 2010, 48(5): 592
9. Gangwar R, Mishra S, Singh V K. Designing of endlessly single mode polarization maintaining highly birefringent nonlinear microstructure fiber at telecommunication window by FV-FEM. Optik-

International Journal for Light and Electron Optics, 2014, 125(5): 1641–1645

10. Olszewski J, Mergo P, Gasior K, Urba'nczyk W. Highly birefringent microstructured polymer fibers optimized for a preform drilling fabrication method. Journal of Optics, 2013, 15(7): 075713

11. Ferrando A, Silvestre E, Andres P, Miret J, Andres M. Designing the properties of dispersion-flattened photonic crystal fibers. Optics Express, 2001, 9(13): 687–697

12. Reeves W, Knight J, Russell P, Roberts P. Demonstration of ultra-flattened dispersion in photonic crystal fibers. Optics Express, 2002, 10(14): 609–613

13. Raja G T, Varshney S K. Large mode area modified clad leakage channel fibers with low bending and higher differential losses. Journal of Optics, 2014, 16(1): 015403

14. Saini T S, Kumar A, Sinha R K. Triangular-core large-mode-area photonic crystal fiber with low bending loss for high power applications. Applied Optics, 2014, 53(31): 7246–7251

15. Saini T S, Kumar A, Sinha R K. Asymmetric large-mode-area photonic crystal fiber structure with effective single-mode operation: design and analysis. Applied Optics, 2016, 55(9): 2306–2311

16. Razzak S A, Namihira Y. Proposal for highly nonlinear dispersion-flattened octagonal photonic crystal fibers. IEEE Photonics Technology Letters, 2008, 20(4): 249–251

17. Gangwar R K, Bhardwaj V, Singh V K. Magnetic field sensor based on selectively magnetic fluid infiltrated dual-core photonic crystal fiber. Optical Engineering (Redondo Beach, Calif.), 2016, 55(2): 026111

18. Dhara P, Singh V K. Effect of MMF stub on the sensitivity of a photonic crystal fiber interferometer sensor at 1550 nm. Optical Fiber Technology, 2015, 21: 154–159

19. Gangwar R K, Singh V K. Refractive index sensor based on selectively liquid infiltrated dual core photonic crystal fibers. Photonics and Nanostructures-Fundamentals and Applications, 2015, 15: 46

20. Musin R, Zheltikov A. Designing dispersion-compensating photonic-crystal fibers using a genetic algorithm. Optics Communications, 2008, 281(4): 567–572

21. Simpson J, Stolen R, Sears F, Pleibel W, MacChesney J, Howard R. A single-polarization fiber. Journal of Lightwave Technology, 1983, 1(2): 370–374

22. Messerly M J, Onstott J R, Mikkelson R C. A broad-band single polarization optical fiber. Journal of Lightwave Technology, 1991, 9 (7): 817–820

23. Okamoto K. Single-polarization operation in highly birefringent optical fibers. Applied Optics, 1984, 23(15): 2638

24. Yang T J, Shen L F, Chau Y F, Sung M J, Chen D, Tsai D P. High birefringence and low loss circular air-holes photonic crystal fiber using complex unit cells in cladding. Optics Communications, 2008, 281(17): 4334–4338

25. Chau Y F, Yeh H H, Tsai D P. Significantly enhanced birefringence of photonic crystal fiber using rotational binary unit cell in fiber cladding. Japanese Journal of Applied Physics, 2007, 46(43 11L): L1048–L1051

26. Chen D, Shen L. Highly birefringent elliptical-hole photonic crystal fibers with double defect. Journal of Lightwave Technology, 2007,

25(9): 2700–2705

27. Sun Y S, Chau Y F, Yeh H H, Shen L F, Yang T J, Tsai D P. High birefringence photonic crystal fiber with a complex unit cell of asymmetric elliptical air hole cladding. Applied Optics, 2007, 46 (22): 5276–5281

28. Islam M A, Alam M S. Design of a polarization-maintaining equiangular spiral photonic crystal fiber for residual dispersion compensation over $E + S + C + L + U$ wavelength bands. IEEE Photonics Technology Letters, 2012, 24(11): 930–932

29. Yue Y, Kai G, Wang Z, Sun T, Jin L, Lu Y, Zhang C, Liu J, Li Y, Liu Y, Yuan S, Dong X. Highly birefringent elliptical-hole photonic crystal fiber with squeezed hexagonal lattice. Optics Letters, 2007, 32(5): 469–471

30. Chaudhuri P R, Paulose V, Zhao C, Lu C. Near-elliptic core polarization-maintaining photonic crystal fiber: modeling birefringence characteristics and realization. IEEE Photonics Technology Letters, 2004, 16(5): 1301–1303

31. Samiul Habib M, Selim Habib M, Hasan M I, Razzak S M A. Highly nonlinear polarization maintaining two zero dispersion spiral photonic crystal fiber using artificial defects. Optical Fiber Technology, 2013, 19(6): 539–542

32. Samiul Habib M, Selim Habib M, Hasan M I, Razzak S M A, Hossain M A, Namihira Y. Polarization maintaining large nonlinear coefficient photonic crystal fibers using rotational hybrid cladding. Optik-International Journal for Light and Electron Optics, 2014, 125 (3): 1011–1015

33. Hasan M I, Mahmud R, Morshed M, Hasan M R. Ultraflattened negative dispersion for residual dispersion compensation using soft glass equiangular spiral photonic crystal fiber. Journal of Modern Optics, 2016, 63(17): 1681–1687

34. Selim Habib M, Samiul Habib M, Razzak S M A, Hossain M A. Proposal for highly birefringent broadband dispersion compensating octagonal photonic crystal fiber. Optical Fiber Technology, 2013, 19 (5): 461–467

35. Suzuki K, Kubota H, Kawanishi S, Tanaka M, Fujita M. Optical properties of a low-loss polarization-maintaining photonic crystal fiber. Optics Express, 2001, 9(13): 676–680

36. Hasan M R, Islam M A, Rifat A A, Hasan M I. A singlemode highly birefringent dispersion-compensating photonic crystal fiber using hybrid cladding. Journal of Modern Optics, 2017, 64(3): 218–225

37. Hasan M I, Selim Habib M, Samiul Habib M, Razzak S M A. Highly nonlinear and highly birefringent dispersion compensating photonic crystal fiber. Optical Fiber Technology, 2014, 20(1): 32–38

38. Chou Chau Y F, Lim C M, Yoong V N, Syafi'ie Idris M N. A simple structure of all circular-air-holes photonic crystal fiber for achieving high birefringence and low confinement loss. Journal of Applied Physics, 2015, 118(24): 243102

39. Yang K Y, Chau Y F, Huang Y W, Yeh H Y, Ping Tsai D. Design of high birefringence and low confinement loss photonic crystal fibers with five rings hexagonal and octagonal symmetry airholes in fiber cladding. Journal of Applied Physics, 2011, 109(9): 093103

40. Md A I. Broadband dispersion compensation of single mode fiber by using modified decagonal photonic crystal fiber having high birefringence. Journal of Lasers Optics & Photonics, 2015, 2: 123

41. Haque M M, Rahman M S, Habib M S, Razzak S. Design and

characterization of single mode circular photonic crystal fiber for broadband dispersion compensation. Optik-International Journal for Light and Electron Optics, 2014, 125(11): 2608–2611

42. Gangwar R K, Singh V K. Study of highly birefringence dispersion shifted photonic crystal fiber with asymmetrical cladding. Optik-International Journal for Light and Electron Optics, 2016, 127(24): 11854–11859

43. Koshiba M. Full-vector analysis of photonic crystal fibers using the finite element method. IEICE Transactions on Electronics, 2002, 85 (4): 881

44. Lee H, Schmidt M, Tyagi H, Sempere L P, Russell P S J. Polarization-dependent coupling to plasmon modes on submicron gold wire in photonic crystal fiber. Applied Physics Letters, 2008, 93 (11): 111102

45. Malitson I. Interspecimen comparison of the refractive index of fused silica. Journal of the Optical Society of America, 1965, 55 (10): 1205

46. Agrawal G P. Fiber-Optic Communication Systems. vol. 222. New York: John Wiley & Sons, 2012

47. Saitoh K, Koshiba M. Full-vectorial imaginary-distance beam propagation method based on a finite element scheme: application to photonic crystal fibers. IEEE Journal of Quantum Electronics, 2002, 38(7): 927–933

48. Caillaud C, Gilles C, Provino L, Brilland L, Jouan T, Ferre S, Carras M, Brun M, Mechin D, Adam J L, Troles J. Highly birefringent chalcogenide optical fiber for polarization-maintaining in the 3–8.5 μm mid-IR window. Optics Express, 2016, 24(8): 7977–7986

49. Chen D, Wu G. Highly birefringent photonic crystal fiber based on a double-hole unit. Applied Optics, 2010, 49(9): 1682–1686

50. Begum F, Namihira Y, Razzak S A, Kaijage S, Hai N H, Kinjo T, Miyagi K, Zou N. Novel broadband dispersion compensating photonic crystal fibers: applications in high-speed transmission systems. Optics & Laser Technology, 2009, 41(6): 679–686

51. Haxha S, Ademgil H. Novel design of photonic crystal fibres with low confinement losses, nearly zero ultra-flatted chromatic dispersion, negative chromatic dispersion and improved effective mode area. Optics Communications, 2008, 281(2): 278–286

52. Lægsgaard J, Libori S B, Hougaard K, Riishede J, Larsen T, Sørensen T, Hansen T P, Hansen K P, Nielsen M D, Jensen J, Bjarklev A. Dispersion properties of photonic crystal fibers-issues and opportunities. MRS Online Proceedings Library Archive, 2003, 797(8): 135–136

53. Luke S, Sudheer S, Pillai V M. Tellurite based circular photonic crystal fiber with high nonlinearity and low confinement loss. Optik-International Journal for Light and Electron Optics, 2016, 127(23): 11138–11142

54. Liu Z, Wu C, Tse M L V, Lu C, Tam H Y. Ultrahigh birefringence index-guiding photonic crystal fiber and its application for pressure and temperature discrimination. Optics Letters, 2013, 38(9): 1385–1387

55. Falkenstein P, Merritt C D, Justus B L. Fused preforms for the fabrication of photonic crystal fibers. Optics Letters, 2004, 29(16): 1858–1860

Rekha Saha completed her B.Sc. Engg. and M.Sc. Engg. degrees in Electronics and Communication Engineering Discipline from Khulna University, Khulna-9208, Bangladesh, in the year of 2015 and 2018, respectively. She secured 1st position both in B.Sc. and M.Sc. in her Discipline. Her research interests are nanophotonics, plasmonics, optical biosensor, and photonic crystal fiber.

Md. Mahbub Hossain received his B.Sc. and M.Sc. Engineering degrees from Electronics and Communication Engineering Discipline, Khulna University, Khulna-9208, Bangladesh, in the year of 2003 and 2014, respectively. Mr. Mahbub is currently a Faculty Member with the Electronics and Communication Engineering Discipline, Khulna University, Bangladesh. His research interests are nanophotonics, plasmonics, optical biosensor, photonic crystal fiber, and wireless communication.

Md. Ekhlasur Rahaman received the B. Sc. Engg. degree in Electronics and Communication Engineering and the M.Sc. Engg. degree also in Electronics and Communication Engineering from Khulna University, Khulna-9208, Bangladesh, in the year of 2015 and 2018, respectively. He was awarded National Science and Technology (NST) Fellowship, Bangladesh for M.Sc. Engg. thesis work. He has published several papers in journals as well as in the proceedings of IEEE flagship/portfolio conferences. His research interests are cloud computing, nanophotonics, plasmonics, optical bio-sensor, photonic crystal fiber, and laser processing of materials.

Himadri Shekhar Mondal received his B. Sc. and M.Sc. degrees in Electronics and Communication Engineering from Khulna University, Bangladesh, in 2015 and 2018, respectively. Himadri does research on optics, opto-electronics, distributed computing and cloud computing.